Wittmann, H., von Blanckenburg, F., Guyot, J. L., Maurice, L., Kubik, P. W. (2009): From source to sink: Preserving the cosmogenic 10Be-derived denudation rate signal of the Bolivian Andes in sediment of the Beni and Mamoré foreland basins. - Earth and Planetary Science Letters, 288, 3-4, 463-474

DOI: 10.1016/j.epsl.2009.10.008.

From source to sink: Preserving the cosmogenic ^{10}Be-derived denudation rate signal of the Bolivian Andes in sediment of the Beni and Mamoré foreland basins

Earth and Planetary Science Letters
doi:10.1016/j.epsl.2009.10.008

H. Wittmann[a,b,1], F. von Blanckenburg[a,b], J.L. Guyot[c], L. Maurice[d,e], & P. W. Kubik[f]

[a]Institut für Mineralogie, Universität Hannover, Callinstr. 3, Hannover, Germany
[b]Present Address: GeoForschungsZentrum Potsdam, Telegrafenberg, Potsdam, Germany
[c]Instituto de Pesquisa para o Desenvolvimento (IRD), CP 7091 Lago Sul, Brasília, Brazil
[d]Université de Toulouse, UPS (SVT-OMP), LMTG, 14 Av. E. Belin, Toulouse, France
[e] IRD, LMTG, 14 Av. E. Belin, Toulouse, France
[f]Laboratory of Ion Beam Physics, ETH Zurich, Zurich, Switzerland

[1]corresponding author: email Wittmann@gfz-potsdam.de
phone: +49 (0) 331-288 2820
fax: +49 (0) 331-288 2852

Abstract

The denudation rate signal of the Bolivian Andes as measured by cosmogenic ^{10}Be in sediment is preserved in the floodplain of adjacent foreland basins even though these basins store the sediment for thousands of years. This conclusion is drawn from comparing published Andean source area denudation rates with new cosmogenic ^{10}Be data as measured in the floodplains of the large Beni and Mamoré basins. For the entire Beni basin including the sediment producing Andes and the vast flooded plains of the foreland, the cosmogenic nuclide-derived denudation rate is 0.45 ± 0.06 mm/yr, while that of the Mamoré basin is 0.55 ± 0.19 mm/yr. By comparison, the respective Andean source areas erode at averaged rates of 0.37 ± 0.06 mm/yr (upper Beni), and at 0.56 ± 0.09 mm/yr (upper Mamoré). We notice a decrease in variability of denudation rate with increasing spatial scale as small-scale processes are averaged out. Sediment mixing within the floodplain damps scatter of nuclide-derived denudation rates picked up in the source area. On the temporal scale, a remarkable agreement between cosmogenic nuclide-derived rates averaging over a few kiloyears with those from fission track dating averaging over millions of years seems to suggest that cosmogenic nuclide-derived denudation rates capture the long-term erosional characteristics of the mountain belt. The sum of these observations suggests that any sample collected along a river traversing a floodplain will yield the denudation rate of the source area. This finding opens the unique possibility of constraining cosmogenic nuclide-derived paleo-sediment budgets for these large basins as the long-term, spatially-averaged denudation rate signal of the sediment-producing area is preserved in sedimentary archives.

Keywords: Denudation; Erosion; Sediment delivery; Cosmogenic nuclides, Cosmogenic ^{10}Be, Bolivian Andes; Beni River floodplain; Mamoré River floodplain

1. Introduction

To date, cosmogenic nuclides in detrital material have been used to determine catchment-wide mountain erosion and weathering rates (Bierman and Nichols, 2004; von Blanckenburg, 2005; Granger and Riebe, 2007). In the past years, the technique has been applied to settings with increasing complexity, such as formerly glaciated basins, basins featuring variable lithology, areas affected by recent land use or variable degrees of tectonic and climatic forcing. Even where these complexities are present, cosmogenic nuclides mostly record robust basin-wide denudation rates when compared to long-term denudation meters measured by fission tracks (Kirchner et al., 2001; Matmon et al., 2003; Wittmann et al., 2007). The question posed here is whether this method can be used to infer basin-wide denudation rates from sediment routed through large depositional settings (Bierman and Steig, 1996; Nichols et al., 2002; Nichols et al., 2005). In such basins, the transport of sediment includes residence in floodplains due to deposition in the floodplain and reincorporation of sediment in the active fluvial system by bank erosion. Wittmann and von Blanckenburg (2009) recently presented a nuclide budget to model the effect of temporary sediment storage in floodplains. This budget was modeled for a variety of settings

including the Beni floodplain. The conclusion of this analysis was that despite significant floodplain storage, the nuclide concentration established in the sediment-producing hinterland (e.g. the Bolivian Andes) is not changed over spatial scales of typical foreland basins. Hence, the denudation rate derivable from these nuclide concentrations will also be preserved.

The essentially pristine floodplains of the upper Amazon basin are an ideal setting to test this hypothesis. The east-draining Andean setting allows interpreting the cosmogenic nuclide-derived denudation rates in terms of dispersal from an area where sediment is actively being produced by weathering on the hillslope to one in which sediment is accumulating. The focus here is on the Beni and the adjoining Mamoré basins; in case of the Beni, a large dataset of cosmogenic nuclide-derived denudation rates is available for the high Bolivian Andes (Safran et al., 2005). For this area, fission track-derived long-term rates of erosion are also available (Safran et al., 2006). For the upper Andean Mamoré basin, we have sampled the principle sediment-providing rivers in order to constrain the mean Andean denudation rate in this region. We will then proceed to present new cosmogenic nuclide-based denudation rates for the floodplains of the Beni, Mamoré, and Madeira Rivers and will assess how much of the denudation signal is preserved during storage and remobilization as sediment moves down these river courses, being entrained and released within the floodplain in numerous cycles.

2. Study area

During late Oligocene to early Miocene times, subsidence-related flexural basins were formed in the Andean foreland (Dumont and Fournier, 1994). One major Amazon foreland basin is the Madeira basin, which is mainly comprised of the Beni (~ 300.000 km^2) and the adjacent Mamoré (~ 600.000 km^2) basin (see Figure 1). The Madeira basin is one of the most important tributaries to the Amazon River in terms of sediment and water discharge (Guyot, 1993; Guyot et al., 1999). The basin can be subdivided into three major morpho-structural units: The Bolivian segment of the Andes where sediment production is high in steep terrains; the Amazon plain featuring vast flooded, low-relief areas at altitudes < 200 m; and the tectonically inactive Brazilian shield that constitutes old Precambrian rocks. Additionally, the Andean area can be subdivided into the high-relief, steeply sloped Andean part and the low-relief Piedmont section, which is also called the Subandean Belt (Dumont and Fournier, 1994; Horton, 1999; Horton and Decelles, 2001).

Downstream of the transition of the sediment-producing Andean source area to that of the depositional floodplain at Rurrenabaque and upstream of its confluence with the Mamoré River, the Beni River has only two larger tributaries: the Madre de Dios River, a river comparable in size to the Beni draining the Peruvian and Bolivian Andes, and the Orthón River that exclusively drains Miocene lowland sediments of the Fitzcarrald Arch formation (Espurt et al., 2007). The Andean part of the Mamoré basin is mainly drained by the Grande and Pirai Rivers in the south where the Andean chain is widest, and by the Chaparé and Ichilo Rivers, which drain the Bolivian Andes at the northern boundary of the Amazon floodplain. The floodplain part of the Mamoré River drains the vast lowland areas of the “Llanos de los Mojos” and is fed by many small low-gradient rivers. About 100 km upstream of Guayaramerin, the Guaporé-Itenez River joins the Mamoré (see Figure 1), a river carrying low sediment loads due to the highly weathered and slowly denuding Precambrian rocks of the Brazilian Shield (Gibbs and Barron, 1983; Hasui and Dealmeida, 1985; Voicu et al., 2001).

In these large, accumulating floodplains of the Beni and Mamoré, present-day rates of sediment deposition are enormous (Guyot, 1993; Guyot et al., 1996; Aalto et al., 2003). From measuring suspended sediment concentrations in the Andean and floodplain Beni basin, Guyot (1993) and Guyot et al. (1996) for example found that about half of the total sediment flux discharged from the Bolivian Andes is deposited in the adjacent Beni foreland basin. In these settings, the Beni and Mamoré Rivers have developed highly active meander river systems with migration rates of up to 30 m/yr (Gautier et al., 2007). High migration rates account for rapid sediment exchange between the river and the floodplain; Dosseto et al. (2006) have estimated a residence time of sediment in the Beni floodplain between Rurrenabaque and the outlet of the Beni floodplain (at its confluence with the Mamoré, see Figure 1) of 4 - 6 kyr by using U-series isotopes. Within this time period, sediment is incorporated into the floodplain and subsequently eroded from the river banks. In general, it is likely that almost all sand and much of the silt and clay in transition through these systems has spent some time stored in the floodplain (Lauer and Parker, 2008).

3. Methods

3.1 Sampling

Where possible, our cosmogenic nuclide sampling of sediment from active fluvial bars was carried out near a gauging monitoring station (see Figure 1); the Beni was sampled during October 2002 and the Mamoré during cruises in July 2001. All samples were collected by J.L. Guyot within the framework of the HYBAM project, a collaboration of the French IRD Institute with South American Institutes and Universities. The upper Andean Beni basin is characterized by sample BE 1 at Rurrenabaque. In the Beni floodplain, our sampling transect covers a distance across the floodplain of about 600 km from Rurrenabaque to Cachuela Esperanza

(samples BE 2 to 17). Tributary input to the Beni is characterized by samples from the rivers Madre de Dios at Miraflores (MD 15), and the Orthón at Caracoles (OR 16). Within the upper Mamoré basin, we have sampled the primary sediment-delivering Andean catchments of the Grande, Pirai, Chaparé, Ichilo, and Maniqui (see Figure 1). The Grande was sampled at Puente Arce within the high Andes (sample GR 25), and again at the Andean-Piedmont transition at Abapo (GR 19). The Pirai River was sampled at Angostura at the Piedmont-floodplain transition. The basins of the Chaparé (CHA 23) and the Ichilo (ICH 21) that drain the northern front of the southern Bolivian Andes were also sampled, although only the Chaparé sample accounts for pure Andean denudation at the immediate Piedmont outlet at Villa Tunari. Sample ICH 21 was taken at Puerto Villarroel, which is situated in the floodplain ~30 km from the Piedmont front, thus 39% of the basin are located in the floodplain. The basin of the Maniqui (MAN 15) drains Sub-Andean terrain east of the upper Beni basin. The Mamoré floodplain was sampled at several localities along the main river (see Figure 1); at Puerto Pailas on the Grande River (GR 17), and at Puerto Ganadero (MAR 16) and Guayaramerin (MAR 18) on the Mamoré River. The latter sample integrates over the cratonic areas of the Brazilian Shield (~ 50% floodplain area; ~ 60% Brazilian Shield area; ~ 10% Andean territory). The Madeira River was sampled at about ~40 km below the Beni-Mamoré confluence (MAD 19) and again at Porto Velho (MAD 20).

3.2 Sample preparation and AMS measurements

Samples were dried and sieved; for ^{10}Be analysis, pure quartz of grain sizes between 125-500 µm was selected. In this study "a" denotes the 125-250 µm and "b" the 250-500 µm grain size fraction (Table 1). ^{10}Be was extracted from purified quartz using standard methods (von Blanckenburg et al., 1996; von Blanckenburg et al., 2004), ^{10}Be/^{9}Be ratios were measured in BeO targets with accelerator mass spectrometry at ETH Zurich relative to the standard S555 with a nominal value of ^{10}Be/^{9}Be = 95.5 $\times 10^{-12}$ and corrected as described by Synal et al. (1997), which is based on a ^{10}Be half life of 1.51 Myr (Hofmann et al., 1987). Between 150 and 300 µg of ^{9}Be carrier was added to each sample, which was determined to contain a ^{10}Be/^{9}Be ratio of $0.55 \pm 0.28 \times 10^{-14}$, except samples denoted by an asterisk in Table 1 that had a higher blank ratio. Analytical as well as blank error corrections are described in Table 1. Calculations of production rates, using pixel-based altitudes from 1 km resolution SRTM-DEM, and attenuation laws including muons were done following Schaller et al. (2002); atmospheric scaling was done following Dunai (2000). Published denudation rates from the high Andes of the Andean Beni basin by Safran et al. (2005) were recalculated for comparison with our dataset; we have recalculated their denudation rates for Dunais´ atmospheric scaling laws and included nuclide production by muons as suggested by Schaller et al. (2002).

3.3. Corrections of basin-wide production rates

Corrections of the production rate due to past variations in the intensity of the Earth's magnetic dipole field were only necessary for sample OR 16b, which has an apparent age of 27 kyr at a basin-averaged latitude of 15°S. Correction amounts to additional 20% in total production due to enhanced dipole intensity according to Gosse and Philips (2001) and Masarik et al. (2001). All other samples are ±10 kyr or younger in age at basin-averaged latitudes of 15°S for the Beni and Mamoré, which means that a correction for dipole variability is not necessary, because the sea level high latitude reference production rate of 5.53 at/g$_{(Qz)}$ (Kubik et al., 1998) used here already incorporates the geomagnetic changes over this period.

3.4 Treatment of cosmogenic nuclide-derived denudation rates and derived sediment fluxes in depositional settings

The conclusion of the model presented by Wittmann and von Blanckenburg (2009) is that in most floodplains, the denudation signal of the sediment source area is preserved by its cosmogenic nuclide concentration, regardless of the duration of temporary storage. This finding is valid if the storage is short compared to the half life of the nuclide. Obviously, the loss of sediment to the floodplain does not alter the nuclide concentration of the sediment remaining in the trunk stream. Importantly, sediment contributed to the trunk stream by erosion of the floodplain adds only a minor additional portion of nuclides. These are those produced within approximately the upper meter of the floodplain, whereas the deeper 15 to 25 m of floodplain contribute shielded sediment that does not change the source area´s nuclide signal when mixed with sediment carried by the trunk stream. Yet, the calculation of a cosmogenic nuclide-derived denudation rate (ε_{cosmo}) requires that the nuclide production rate is scaled to the altitude of the sediment producing area. Because not all catchment area located upstream of a sampling point within a floodplain is actually producing sediment, we calculate floodplain-corrected cosmogenic nuclide-based denudation rates (termed ε_{FC} in the following) (Wittmann and von Blanckenburg, 2009). To this end, all basin-averaged denudation rates of which the catchment contains a floodplain area are corrected by defining a "floodplain-corrected" sediment source area A_{FC}. A_{FC} contributes actively produced sediment and excludes lowland area where sediment is mostly deposited.

For the Beni basin, this transition is located at the city of Rurrenabaque. In the Mamoré basin, no hinterland area common to all samples can be defined, thus we used a 1 km resolution SRTM elevation model set to a cut-off altitude of 400 m. We then proceeded to calculate an average SRTM pixel-based floodplain-corrected cosmogenic production rate (P_{FC}) that is limited to the area contributing sediment in the respective basin (see Table 1). Solving Lal´s (1991) equation for a uniform floodplain-corrected denudation rate ε_{FC} (mm/yr), one obtains the following simplified equation:

$$\varepsilon_{FC} = \left(\frac{P_{FC}}{\rho \times C} - \lambda\right) \times \Lambda \quad (1)$$

where for simplicity the equation is shown with P_{FC} containing all nucleogenic and muonic production mechanisms. The nuclide concentration C (at/$g_{(Qz)}$) is measured in quartz from sediment samples, λ is the decay constant (1/yr), Λ is a mean cosmic ray attenuation length (g/cm^2) including nucleons and muons, and ρ is the density of rock (g/cm^3).

Weighting a cosmogenic nuclide-derived denudation rate by its sediment load becomes necessary whenever an averaged cosmogenic nuclide concentration or denudation rate, respectively, is calculated for a trunk stream from those of individual sub-basins (e.g. in the Mamoré basin). Our cosmogenic nuclide-based denudation rates ε_{cosmo} are weighted by the respective sediment load (Q_{cosmo}, t/yr), which can be calculated according to:

$$Q_{\cos mo} = F_{\cos mo} \times A_{basin} \quad (2)$$

where F_{cosmo} (t/km^2/yr) is calculated from ε_{cosmo} (mm/kyr) × ρ (t/km^3) and A_{basin} gives the total drainage area (km^2). A flux-weighted denudation rate $\overline{\varepsilon}$ (mm/yr) results as smaller basins contribute less sediment than larger basins:

$$\overline{\varepsilon} = \frac{\sum_{i=1}^{n} \left(Q_{i\cos mo} \times \varepsilon_{i\cos mo}\right)}{\sum_{i=1}^{n} Q_{i(\cos mo)}} \quad (3)$$

In the Mamoré floodplain, a floodplain-corrected and flux-weighted denudation rate $\overline{\varepsilon}_{FC}$ is calculated by weighting ε_{FC} of the trunk stream by each Q_{cosmo} of the individual sub-basins, simply by substituting ε_{FC} for ε_{cosmo} in Equation 3.

3.5 Treatment of gauging-derived sediment yields in depositional settings

For the Beni and Mamoré basins, modern denudation rates from sediment gauging and dissolved element measurements are available for several decades (Table 2). This database covers the area from the Bolivian Andes down to the floodplain of the rivers under investigation here. In large lowland basins, sediment yields (termed F_M in the following, and calculated by taking the measured Q_M (t/yr) of a basin divided by A_{basin} (km^2)) decrease with increasing basin size if no new sediment is added downstream (e.g. (Milliman and Meade, 1983; Milliman and Syvitski, 1992; Hovius, 1998)). This effect arises even if no sediment is deposited in the floodplain and the sediment discharge Q_M is uniform throughout the floodplain. If the sediment yield is used to calculate denudation rates of the areas actually producing sediment, a correction of this effect is necessary. Thus, similarly to the treatment cosmogenic nuclide-derived denudation rates are subjected to, published gauging-derived sediment yields F_M (see Table 2) were corrected for floodplain area according to:

$$F_{FC} = \frac{Q_M}{A_{FC}} \quad (4)$$

where F_{FC} is the floodplain-corrected sediment yield of a basin (see Table 2), and A_{FC} is the sediment-producing area which is determined as described in Section 3.4 for cosmogenic nuclide production rates . Similar to our terminology for cosmogenic nuclide-based denudation rates, we term “modern” denudation rates calculated from sediment yields ε_M, and floodplain-corrected modern denudation rates ε_{MFC}.

The total sediment load that is discharged from the Andes to the Beni floodplain passing Rurrenabaque amounts from 220 Mt/yr (Guyot et al., 1996) to 300 Mt/yr (Maurice-Bourgoin et al., 2002; see Table 2), which corresponds to a modern denudation rate range of 1.18 to 1.63 mm/yr. Downstream in the floodplain at Riberalta gauging station, this flux decreases strongly to ~120 Mt/yr (corresponds to an ε_{MFC} of 0.71 mm/yr, see Table 2), indicating net sediment deposition. At Cachuela Esperanza downstream of the Orthón and Madre de Dios confluences, ε_{MFC} is with 1.15 mm/yr again in the same range as at Rurrenabaque; this increase is attributed to the high sediment input from the Madre de Dios River.

The main sediment provider to the Mamoré floodplain is the Grande River; its modern load Q_M amounts to ~ 140 Mt/yr (Guyot et al., 1996) at the Andean outlet at Abapo, which corresponds to an ε_M of 0.89 mm/yr. In the Mamoré floodplain, this denudation rate decreases to ε_{MFC} = 0.22 mm/yr at Puerto Ganadero, ~ 400 km downstream from Abapo, and to 0.18 mm/yr at Puerto Siles, respectively. At the outlet of the Mamoré floodplain at Guyaramerin, the total recorded flux of ~80 Mt/yr (0.25mm/yr) is about half of the recorded Andean Grande sediment flux, also indicating net sediment loss to the floodplain.

Uncertainties associated with this method are difficult to assess and their accuracy, precision and general reliability have been subject to intense debate (e.g. (Bransky, 1981; Walling and Webb, 1981; Smith and Croke, 2005)). We therefore attribute no general uncertainty on sediment loads, but the reader should be aware that associated errors normally range between 10-50% (e.g. (Martinelli et al., 1989; Guyot et al., 1996; Métivier and Gaudemer, 1999)), but strongly depend on the individual study and methods used therein.

4. Cosmogenic ^{10}Be-derived denudation rates and their interpretation

4.1 Source area denudation rates in the Andes

4.1.1 The upper Beni basin

At the transition from the Andes to the floodplain at Rurrenabaque, measured cosmogenic nuclide-derived denudation rates ε_{cosmo} result in an average rate of 0.37 ± 0.06 mm/yr from the two grain size measurements of BE 1a and 1b (see Table 1). This denudation rate should average over the entire upper Beni basin, including the Andean and Piedmont section. At the same location, Safran et al. (2005) have also determined a cosmogenic nuclide-based denudation rate. The respective recalculated denudation rate for sample BOL-50 (Safran et al., 2005) amounts to 0.55 ± 0.03 mm/yr. The observed difference in denudation rates at Rurrenabaque (resulting from different nuclide concentrations when taking the same production rate for denudation rate calculation) can potentially be attributed to temporal variability of source areas providing sediment. For example, the higher denudation rate measured at Rurrenabaque by Safran et al. (2005) might be indirectly induced by a stronger ENSO event during the sampled year, producing large landslides in the Piedmont region at elevations below 3000 m (Blodgett and Isacks, 2007). In addition to temporal variations, we cannot exclude the possibility of spatial variations in erosion sources in the Bolivian Andes. For example, stream sediment in the upper Beni basin can vary in the mixing proportions of sediment sourced in the high-relief, steeply sloped Andean part and the low-relief Piedmont section. For the Piedmont region, no ε_{cosmo} data is available. The dataset from Safran et al. (2005) documents the high spatial variability of denudation rates present in the high Bolivian Andes; the mean denudation rate amounts to 0.36 mm/yr with a standard deviation of 0.22 mm/yr. The flux-weighted mean for this area amounts to 0.43 ± 0.03 mm/yr (Eq. 3), which compares reasonably well to our denudation rate measured at Rurrenabaque.

4.1.2 The upper Mamoré basin

Within the upper Mamoré basin, the primary sediment-delivering Andean catchments analyzed yield highly variable cosmogenic nuclide-derived denudation rates. The Andean basin of the Grande (sample GR 25a) erodes at a rate of 0.13 ± 0.01 mm/yr, whereas at the Andean-Piedmont transition (GR 19b), a much higher ε_{cosmo} of 0.63 ± 0.09 mm/yr was recorded. The Pirai River basin erodes at a similar rate of 0.47 ± 0.16 mm/yr (average from PIR 18b and 18c). The basin of the Chaparé (CHA 23a) yields an ε_{cosmo} of 0.26 ± 0.03 mm/yr, and the Ichilo (ICH 21a) denudation rate amounts to 0.33 ± 0.07 mm/yr. Since this sample was taken some distance away from the transition between the Piedmont and the floodplain, this erosion signal may not be purely Andean. The basin of the Maniqui (MAN 15b) erodes at a cosmogenic nuclide-derived denudation rate of 0.49 ± 0.11 mm/yr. For means of comparison with floodplain denudation rates, a calculation of a flux-weighted Andean denudation rate for these basins is necessary. For the Grande, Pirai, Chaparé, Ichilo, and Maniqui basins, $\overline{\varepsilon}$ (see Eq. 3) amounts to 0.56 ± 0.09 mm/yr, resulting in an averaged integration time scale for erosion of ~1.2 kyr.

We can compare our cosmogenic nuclide-derived denudation rates with those measured by Insel et al. (2007), who have measured sub-basins of the Grande, too, but also more southern basins of the Pilcomayo and Parapeti Rivers. Their preliminary denudation rates cover a range from 0.04 to 1.93 mm/yr for basins ranging from 4 to 5200 km^2 in drainage area (N. Insel, pers. comm., 2009).

4.2 Denudation rates measured in floodplains

4.2.1 The Beni River floodplain

For 600 km of floodplain within the Beni River basin from Rurrenabaque to Cachuela Esperanza, mean nuclide concentrations are $3.7 \pm 0.5 \times 10^4$ at/g$_{(Qz)}$ (BE 2 to 17, n = 12, excluding tributaries; also see Wittmann and von Blanckenburg, 2009). This concentration compares well to that obtained from BE 1 at Rurrenabaque ($3.8 \pm 0.6 \times 10^4$ at/g$_{(Qz)}$). The detection of similar nuclide concentrations for both the upstream sample at Rurrenabaque and the samples along the entire floodplain (see Figure 2) leads us to assume that the initial nuclide concentration discharged from the upper Beni basin is indeed not altered over the length of the floodplain, despite very rapid river migration rates causing frequent sediment exchange between the channel and the floodplain. We therefore recalculated the denudation rates for the Beni River floodplain according to Section 3.4 to include the sediment-producing areas only (ε_{FC}, see Eq. 1) following Wittmann and von Blanckenburg (2009). Results from this recalculation give an average floodplain denudation rate ε_{FC} of 0.45 ± 0.06 mm/yr that is very similar to our denudation rate estimate at Rurrenabaque (0.37 ± 0.06 mm/yr). With a rate of 0.28 ± 0.13 mm/yr, the tributary input from the Madre de Dios River is comparable to the Beni erosion signal. The Orthón River however is with an ε_{cosmo} of 0.033 ± 0.004 mm/yr clearly distinguishable from the Beni. The Orthón basin does not receive fresh, unweathered Andean sediment and denudation rates within the basin are slow. Admixing from high-nuclide concentrated Orthón sediment is not changing the Beni mainstream mixed nuclide concentration.

4.2.2 The Mamoré River floodplain

For the Mamoré River, tracing sediment from source to sink as in the Beni is not possible, as this river has many larger tributaries of which some drain either floodplain areas only, or slowly eroding Brazilian shield areas in the lower reaches. For this reason, the following denudation rates are corrected for floodplain area (ε_{FC}) and average floodplain rates are also flux-weighted (the combination is termed $\overline{\varepsilon}_{FC}$, see Section 3.4).

Denudation rates ε_{FC} in the Grande - Mamoré floodplain range from 0.51 ± 0.09 mm/yr (GR 17b) to 0.85 ± 0.31 mm/yr (MAR 16, n = 2; see Table 1). Although being within uncertainty of the Andean mean ($\overline{\varepsilon}$ = 0.56 ± 0.09 mm/yr), the observed increase in denudation rate along the floodplain could be explained by addition of sediment containing low nuclide concentrations due to bank erosion in the floodplain. This possibility would require deep floodplain storage for very long periods (several Myr) in order for nuclides to decay from their original nuclide composition. However, Mamoré migration rates are comparable to those of the Beni River (Gautier et al., 2007), which means that sediment residence times do not exceed those observed in the Beni River case. Channel depths are only ~ 10 m, which makes the incorporation of deeply stored floodplain sediment to the main channel relatively unlikely. Since modern gauging-based sediment fluxes record deposition, not erosion (see Section 3.5), and denudation rates in the Mamoré Andean hinterland probably are spatially highly variable (Insel et al., 2007), we are confident that the measured denudation rate for the Mamoré floodplain represents within scatter the source area signal of the Bolivian Andes. Further downstream in the Mamoré floodplain near Guayaramerin, denudation rates (ε_{FC}) decrease to 0.19 ± 0.06 mm/yr (avg. from MAR 18-1 and 18-2). This decrease in denudation with respect to the Andean mean is attributed to sediment input with high nuclide concentrations from cratonic areas drained by the Guaporé that denude at very low rates. Wittmann (2008) has measured several subbasins of the Brazilian Shield including the Guaporé basin, and average denudation rates are low at 0.02 mm/yr.

For the total Mamoré floodplain, $\overline{\varepsilon}_{FC}$ from samples GR 17, MAR 16 and 18 calculated to minimize bias possibly introduced from differently sized subbasins amounts to 0.55 ± 0.19 mm/yr (see Figure 4). The relatively high uncertainty results from the high sample-specific scatter due to high natural variability; analytical scatter of the individual samples is usually less than 20% (see Table 1).

4.2.3 The Madeira River floodplain

The denudation rate for the Madeira basin including the Beni and Mamoré basins amounts to 0.28 ± 0.04 mm/yr. This rate is lower than average Andean rates derived from the mean Beni denudation rate at Rurrenabaque (0.37 ± 0.06 mm/yr) and the one calculated for the southern Mamoré Andes (0.56 ± 0.09 mm/yr, $\overline{\varepsilon}_{FC}$, calculated from MAD 19a, 20a-1 and 2). This decrease is probably caused by high-nuclide concentration input from the Guaporé basin, similar to what has been observed near Guayaramerin (see Section 4.2). The Guaporé River mostly drains the Brazilian shield, an area of high long-term geomorphic stability featuring old Precambrian rocks that evidently erode at very slow rates (Wittmann, 2008).

5. Implications

5.1 Comparison between cosmogenic nuclide-derived and published gauging-derived denudation rates

Modern denudation rates (ε_{MFC}) for the Beni floodplain are with a mean rate of ~1 mm/yr (Table 2) significantly higher than the mean cosmogenic nuclide-derived rate (ε_{FC} = 0.45 mm/yr). This difference probably stems from the different integration time scales of both methods. In the Beni, our cosmogenic nuclide measurements record the time-integrated signal of denudation for the last ~2.4 kyr, whereas sediment gauging data integrates over the gauging period, which is typically ~ 10 yr (see Table 2). An increase in modern denudation rates can be attributed to changes in land use (Vanacker et al., 2007) or climate (Abbott et al., 1997; Cross et al., 2000) in the sediment-providing area. In this case our new cosmogenic nuclide-derived rates provide the background erosion signal of the last few kiloyears prior, for example, extensive human modifications.

In the Mamoré floodplain, the reverse situation is present; cosmogenic nuclide-based denudation rates ($\bar{\varepsilon}_{FC}$ = 0.55 mm/yr) exceed those recorded by modern loads (~0.2 mm/yr for the Mamoré River, see Table 2). We consider it being relatively unlikely that a removal of deeply shielded floodplain material adds scatter to our cosmogenic nuclide concentrations, as modern loads record floodplain deposition, not erosion. A time scale issue may be the cause for the observed discrepancy, because in the dry Andean hinterland of the Mamoré, sediment transport efficiency is low on decadal scales (an effect noticed by Kober et al. (2009) in the arid setting of the Rio Lluta on the western side of the Andes). Within the longer time scales of cosmogenic nuclides, however, transport efficiency may be higher. In the wetter Beni basin, decadal-scale erosion processes are not limited by transport efficiency. Additionally, the observed difference between both methods in the Mamoré basin can be attributed to high erosional variability in the small basins of the Andean sediment source areas. We will show in the next section that scatter in cosmogenic nuclide-derived denudation rates evidently is reduced as basin sizes increase and cosmogenic denudation rates approach the value of long-term fission track estimates.

5.2 Extending the temporal and spatial scales in denudation

Figure 4 summarizes all cosmogenic nuclide-derived denudation rate data for specific regions in the Beni and Mamoré basins as discussed in Section 4. In the following, we will discuss the significance of the observed erosion patterns in terms of more general issues, e.g. (1) latitudinal orographic effects, (2) temporal uniformity in denudation, and (3) the possibility of extending the spatial scale of cosmogenic-derived denudation meters from the source area to depositional floodplain settings.

(1) Comparing Andean denudation rates obtained from the upper Mamoré and Beni basins, our Mamoré denudation rates are slightly higher than those recorded in the upper Beni. From this, an orographically-controlled latitudinal variation as suggested by Barnes and Pelletier (2006) from various erosion meters for this region of the Andes could tentatively be inferred. For example, an orographically-controlled pattern of rainfall that is also reflected in the pattern of denudation has been observed for the western sides of Andes in northern Chile (Kober et al., 2007). In our view however, the difference observed for the Beni and Mamoré basins is not sufficiently pronounced to deduce a precipitation-related denudation control. Temporal variability introduced may translate into the observed spatial pattern in denudation as it does in the Beni catchment (see Section 4.1.1), an effect that must not be coupled to variations in precipitation but rather to the local hillslope setting.

(2) Long-term denudation rates derived from fission-track analyses are available for the upper Beni basin and integrate over long time scales from 5 to 20 Myr. Observed rates are between 0.2 - 0.6 mm/yr and average at ~ 0.3 mm/yr (Safran et al., 2006). An exponential increase in exhumation rate at 10 - 15 Myr from 0.2 to ~ 0.7 mm/yr has also been suggested for this area by Benjamin et al. (1987) and Anders et al. (2002). If these fission track-derived rates contain a long wavelength signal of mountain building and are no local features, comparison to the integrated denudation signal of the upper Beni basin is a worthwhile exercise. This comparison shows close similarity between denudation rates obtained from these two methods. This finding is surprising, given that the Holocene period over which cosmogenic nuclides record denudation is not necessarily representative for the Quaternary and Pliocene climate for which fission track data is representative. Yet this observation has been made elsewhere (Kirchner et al., 2001; Matmon et al., 2003; Wittmann et al., 2007) in totally diverse settings in terms of climatic and tectonic boundary conditions. It is intriguing to note that similarities for such different settings exist, even though we are far from understanding them completely.

(3) In the high Andes of the Beni basin, denudation rates recorded by cosmogenic nuclides are subjected to strong spatial scatter; primary control on denudation is exerted by channel steepness according to Safran et al. (2005). With increasing basin size however, the observed scatter seems to be averaged out (see Figure 5), and average denudation rates are similar for all basin sizes. For Andean basins < 1000 km^2, denudation rates ($\bar{\varepsilon}$) denote to 0.47 ± 0.03 mm/yr and to 0.42 ± 0.03 mm/yr for basins between 1000 - 11,000 km^2, respectively

(recalculated from Safran et al., 2005, as described in Section 3.2 and Eq. 3). Floodplain basins > 70,000 to ~ 300,000 km^2 average to 0.45 ± 0.06 mm/yr (ε_{FC}, samples BE 2 to 17). This signal is again similar to the long-term erosional signal of ~0.3 mm/yr from fission tracks. An explanation for this uniformity may lie in the ability of the system to buffer against changing sediment supply discharged from the source area as caused, for example, by climatic or tectonic perturbations. Continuous storage and remobilization of alluvium via lateral channel migration in the floodplain damps these effects on > millennial time scales, resulting in long floodplain response times relative to shorter-lived climatic or tectonic perturbations (Métivier and Gaudemer, 1999; Phillips, 2003).

These findings open up the possibility of extending the spatial scale of denudation rate measurements to samples taken from streams within large floodplains. In such large depositional basins, the denudation signal from the sediment-providing area is not only preserved, but also will a sample collected at any point along the river course from within the active floodplain channel yield an average denudation rate of the source area.

6. Conclusions

Denudation rates measured from cosmogenic nuclide concentrations in the floodplains of the Beni and Mamoré River basins (Bolivia) are identical to those obtained from the sediment-providing Bolivian Andes. Floodplain storage of sediment at time scales longer than the integration times of the cosmogenic nuclide method does not alter cosmogenic nuclide concentrations, which indicates that a sample collected at any point along the river course from the active floodplain channel will yield an average denudation rate of the source area. In addition, we notice that denudation rates show large variability in the Andes, but small variability in the floodplain while average rates are similar. This indicates that denudation rates converge to a spatially-averaged erosion signal in the floodplain which is insensitive to local effects of mass transport in the source area. On the temporal scale, cosmogenic nuclide-derived denudation rates in the floodplain resemble those from long-term Andean fission track analysis, which hints at a stable fluvial transport system on comparable time scales. These findings allow to suggest that cosmogenic nuclides are the method of choice for tracing denudation rate signals over large floodplain distances. Denudation rates of the sediment-producing areas are being conserved as spatially and temporally averaged signals, and short-term spatial or temporal changes are dampened-out. We thus suggest that sedimentary sequences deposited in floodplains, similar to paleo-denudation rates measured in terrace deposits, record potential integrated time series of past hinterland denudation processes that could be accessed by using cosmogenic nuclides.

Acknowledgements

The authors want to thank Liz Safran for providing her data and for numerous discussions. Jane K. Willenbring is acknowledged for help with calculating production rates. We sincerely thank Anthony Dosseto and Fritz Schlunegger for thoughtful reviews and Kevin P. Norton for comments on an earlier version of this manuscript.

References

Aalto, R., Maurice-Bourgoin, L., Dunne, T., Montgomery, D.R., Nittrouer, C.A., Guyot, J.L., 2003. Episodic sediment accumulation on Amazonian flood plains influenced by El Nino/Southern Oscillation. Nature. 425, 493-497.

Abbott, M.B., Seltzer, G.O., Kelts, K., Southon, J., 1997. Holocene Paleohydrology of the Tropical Andes from Lake Records. Quaternary research. 47, 70-80.

Anders, M.H., Gregory-Wodzicki, K.M., Spiegelman, M., 2002. A critical evaluation of late tertiary accelerated uplift rates for the Eastern Cordillera, central Andes of Bolivia. Journal of Geology. 110, 89-100.

Barnes, J.B., Pelletier, J.D., 2006. Latitudinal variation of denudation in the evolution of the Bolivian Andes. Am J Sci. 306, 1-31.

Benjamin, M.T., Johnson, N.M., Naeser, C.W., 1987. Recent rapid uplift in the Bolivian Andes: Evidence from fission-track dating. Geology. 15, 680-683.

Bierman, P., Steig, E.J., 1996. Estimating rates of denudation using cosmogenic isotope abundances in sediment. Earth Surface Processes and Landforms. 21, 125-139.

Bierman, P.R., Nichols, K.K., 2004. Rock to sediment - Slope to sea with Be-10 - Rates of landscape change. Annual Review of Earth and Planetary Sciences. 32, 215-255.

Blodgett, T.A., Isacks, B.L., 2007. Landslide erosion rate in the Eastern Cordillera of Northern Bolivia. Earth Interactions. 11, 1-30.

Bransky, J., 1981. Accuracy of the variability of suspended sediment measurements, in: Erosion and Sediment Transport Measurement. IAHS Publication, 133, 213-218.

Cross, S.L., Baker, P.A., Seltzer, G.O., Fritz, S.C., Dunbar, R.B., 2000. A new estimate of the Holocene lowstand level of Lake Titicaca, central Andes, and implications for tropical palaeohydrology. Holocene. 10, 21-32.

Dosseto, A., Bourdon, B., Gaillardet, J., Maurice-Bourgoin, L., Allegre, C.J., 2006. Weathering and transport of sediments in the Bolivian Andes: Time constraints from uranium-series isotopes. Earth and Planetary Science Letters. 248, 759-771.

Dumont, J.-F., Fournier, M., 1994. Geodynamic environment of Quaternary morphostructures of the Subandean foreland basins of Peru and Bolivia: characteristics and study methods. Quaternary International. 21, 129-142.

Dunai, T.J., 2000. Scaling factors for production rates of in situ produced cosmogenic nuclides: a critical reevaluation. Earth and Planetary Science Letters. 176, 157-169.

Espurt, N., Baby, P., Brusset, S., Roddaz, M., Hermoza, W., Regard, V., Antoine, P.-O., Salas-Gismondi, R., Bolanos, R., 2007. How does the Nazca Ridge subduction influence the modern Amazonian foreland basin? Geology. 35, 515-518.

Gautier, E., Brunstein, D., Vauchel, P., Roulet, M., Fuertes, O., Guyot, J.L., Darozzes, J., Bourrel, L., 2007. Temporal relations between meander deformation, water discharge and sediment fluxes in the floodplain of the Rio Beni (Bolivian Amazonia). Earth Surface Processes and Landforms. 32, 230-248.

Gibbs, A.K., Barron, C.N., 1983. The Guiana Shield reviewed. Episodes. 1983, 7-14.

Gosse, J.C., Phillips, F.M., 2001. Terrestrial in situ cosmogenic nuclides: theory and application. Quaternary Science Reviews. 20, 1475-1560.

Granger, D.E., Riebe, C.S., 2007. Cosmogenic nuclides in weathering and erosion, in: Drever, J.I., (Ed), Treatise on Geochemistry. Surface and Ground Water, Weathering, and Soils, 5, London.

Guyot, J.L., 1993. Hydrogéochimie des fleuves de l´Amazonie Bolivienne, Ph.D. Thesis, Bordeaux I, Bordeaux, France.

Guyot, J.L., Filizola, N., Quintanilla, J., Cortez, J., 1996. Dissolved solids and suspended sediment yields in the Rio Madeira basin, from the Bolivian Andes to the Amazon, in: Proceedings of the Exeter Symposium. IAHS Publication, 236, 55-63.

Guyot, J.L., Jouanneau, J.M., Wasson, J.G., 1999. Characterisation of river bed and suspended sediments in the Rio Madeira drainage basin (Bolivian Amazonia). Journal of South American Earth Sciences. 12, 401-410.

Hasui, Y., Dealmeida, F.F.M., 1985. The Central Brazil Shield reviewed. Episodes. 8, 29-37.

Hewawasam, T., von Blanckenburg, F., Schaller, M., Kubik, P., 2003. Increase of human over natural erosion rates in tropical highlands constrained by cosmogenic nuclides. Geology. 31, 597-600.

Hofmann, H.J., Beer, J., Bonani, G., Vongunten, H.R., Raman, S., Suter, M., Walker, R.L., Wolfli, W., Zimmermann, D., 1987. Be-10 - Half-life and AMS-Standards. Nuclear Instruments & Methods in Physics Research Section B-Beam Interactions with Materials and Atoms. 29, 32-36.

Horton, B., 1999. Erosional control on the geometry and kinematics of thrust belt development in the central Andes. Tectonics. 18, 1292-1304.

Horton, B., Decelles, P., 2001. Modern and ancient fluvial megafans in the foreland basin system of the Central Andes, southern Bolivia: Implications for drainage network evolution of fold thrust belts. Basin Research. 13, 43-63.

Hovius, N., 1998. Controls on sediment supply by large rivers, in: Shanley, K.W., McCabe, P.J., (Eds), Relative role of eustasy, climate, and tectonism in continental rocks. Society for Sedimentary Geology Special Publication (SEPM), 59, Tulsa, Oklahoma, pp. 3-16.

Insel, N., Ehlers, T.A., Schaller, M., 2007. Sensitivity of denudation rates to latitudinal and orographic variations in climate, Central Andes, Bolivia., in: Fall AGU. Eos Transactions AGU, 88 (52).

Kirchner, J.W., Finkel, R.C., Riebe, C.S., Granger, D.E., Clayton, J.L., King, J.G., Megahan, W.F., 2001. Mountain erosion over 10 yr, 10 k.y., and 10 m.y. time scales. Geology. 29, 591-594.

Kober, F., Ivy-Ochs, S., Schlunegger, F., Baur, H., Kubik, P.W., Wieler, R., 2007. Denudation rates and a topography-driven rainfall threshold in northern Chile: Multiple cosmogenic nuclide data and sediment yield budgets. Geomorphology. 83, 97-120.

Kober, F., Ivy-Ochs, S., Zeilinger, G., Schlunegger, F., Kubik, P.W., Baur, H., Wieler, R., 2009. Complex multiple cosmogenic nuclide concentration and histories in the arid Rio Lluta catchment, northern Chile. Earth Surface Processes and Landforms. 34, 398-412.

Kubik, P.W., Ivy-Ochs, S., Masarik, J., Frank, M., Schluchter, C., 1998. Be-10 and Al-26 production rates deduced from an instantaneous event within the dendro-calibration curve, the landslide of Kofels, Otz Valley, Austria. Earth and Planetary Science Letters. 161, 231-241.

Lal, D., 1991. Cosmic ray labeling of erosion surfaces: in situ nuclide production rates and erosion models. Earth and Planetary Science Letters. 104, 424-439.

Lauer, J.W., Parker, G., 2008. Net local removal of floodplain sediment by river meander migration. Geomorphology. 96, 123-149.

Martinelli, L.A., Victoria, R.L., Devol, A.H., Richey, J.E., Forsberg, B.R., 1989. Suspended sediment load in the Amazon basin: An overview. GeoJournal. 19, 381-389.

Masarik, J., Frank, M., Schafer, J.M., Wieler, R., 2001. Correction of in situ cosmogenic nuclide production rates for geomagnetic field intensity variations during the past 800,000 years. Geochimica Et Cosmochimica Acta. 65, 2995-3003.

Matmon, A., Bierman, P.R., Larsen, J., Southworth, S., Pavich, M., Caffee, M., 2003. Temporally and spatially uniform rates of erosion in the southern Appalachian Great Smoky Mountains. Geology. 31, 155-158.

Maurice-Bourgoin, L., Aalto, R., Guyot, J., 2002. Sediment-associated mercury distribution within a major Amazon tributary: Century-scale contamination history and importance of flood plain accumulation, in: The Structure, Function and Management Implications of Fluvial Sedimentary Systems. IAHS Publication, 276, 161-168.

Métivier, F., Gaudemer, Y., 1999. Stability of output fluxes of large rivers in South and East Asia during the last 2 million years: implications on floodplain processes. Basin Research. 11, 293-303.

Milliman, J., Meade, R.H., 1983. World-wide delivery of river sediment to the oceans. Journal of Geology. 91, 1-21.

Milliman, J.D., Syvitski, J.P.M., 1992. Geomorphic tectonic control of sediment discharge to the ocean- The importance of small mountainous rivers. Journal of Geology. 100, 525-544.

Nichols, K.K., Bierman, P.R., Caffee, M., Finkel, R., Larsen, J., 2005. Cosmogenically enabled sediment budgeting. Geology. 33, 133-136.

Nichols, K.K., Bierman, P.R., Hooke, R.L., Clapp, E.M., Caffee, M., 2002. Quantifying sediment transport on desert piedmonts using 10Be and 26Al. Geomorphology. 45, 105-125.

Phillips, J.D., 2003. Alluvial storage and the long-term stability of sediment yields. Basin Research. 15, 153-163.

Safran, E.B., Bierman, P., Aalto, R., Dunne, T., Whipple, K.X., Caffee, M., 2005. Erosion rates driven by channel network incision in the Bolivian Andes. Earth Surface Processes and Landforms. 30, 1007-1024.

Safran, E.B., Blythe, A., Dunne, T., 2006. Spatially variable exhumation rates in orogenic belts: An Andean example. Journal of Geology. 114, 665-681.

Schaller, M., von Blanckenburg, F., Veldkamp, A., Tebbens, L.A., Hovius, N., Kubik, P.W., 2002. A 30 000 yr record of erosion rates from cosmogenic Be-10 in Middle European river terraces. Earth and Planetary Science Letters. 204, 307-320.

Smith, C., Croke, B., 2005. Sources of uncertainty in estimating suspended sediment load, in: Proceedings of symposium S1 held during the 7th IAHS Scientific Assembly at Foz do Iguaco, Brazil. IAHS Publication, 292, 136-143.

Synal, H.A., Bonani, G., Dobeli, M., Ender, R.M., Gartenmann, P., Kubik, P.W., Schnabel, C., Suter, M., 1997. Status report of the PSI/ETH AMS facility. Nuclear Instruments & Methods in Physics Research Section B-Beam Interactions with Materials and Atoms. 123, 62-68.

Vanacker, V., von Blanckenburg, F., Govers, G., Molina, A., Poesen, J., Deckers, J., Kubik, P., 2007. Restoring dense vegetation can slow mountain erosion to near natural benchmark levels. Geology. 35, 303-306.

Voicu, G., Bardoux, M., Stevenson, R., 2001. Lithostratigraphy, geochronology and gold metallogeny in the northern Guiana Shield, South America: a review. Ore Geology Reviews. 18, 211-236.

von Blanckenburg, F., 2005. The control mechanisms of erosion and weathering at basin scale from cosmogenic nuclides in river sediment. Earth and Planetary Science Letters. 237, 462-479.

von Blanckenburg, F., Belshaw, N., O´Nions, R.K., 1996. Separation of Be-9 and cosmogenic Be-10 from environmental materials and SIMS isotope dilution analysis. Chemical Geology. 129, 93-99.

von Blanckenburg, F., Hewawasam, T., Kubik, P.W., 2004. Cosmogenic nuclide evidence for low weathering and denudation in the wet, tropical highlands of Sri Lanka. Journal of Geophysical Research-Earth Surface. 109.

Walling, D.E., Webb, B., 1981. The reliability of suspended sediment load data, in: Erosion and Sediment Transport Measurement. IAHS Publication, 133, 177-194.

Wittmann, H., 2008. New applications to in situ-produced cosmogenic nuclides in river sediment: High mountain belt denudation in the Swiss Alps and Bolivian Andes and sediment transfer and storage in the Amazon basin, Ph.D. Thesis, University of Hannover, Hannover, Germany.

Wittmann, H., von Blanckenburg, F., 2009. Cosmogenic nuclide budgeting of floodplain sediment transfer. Geomorphology. 109, 246-256.

Wittmann, H., von Blanckenburg, F., Kruesmann, T., Norton, K.P., Kubik, P.W., 2007. Relation between rock uplift and denudation from cosmogenic nuclides in river sediment in the Central Alps of Switzerland. Journal of Geophysical Research-Earth Surface. 112.

Figures

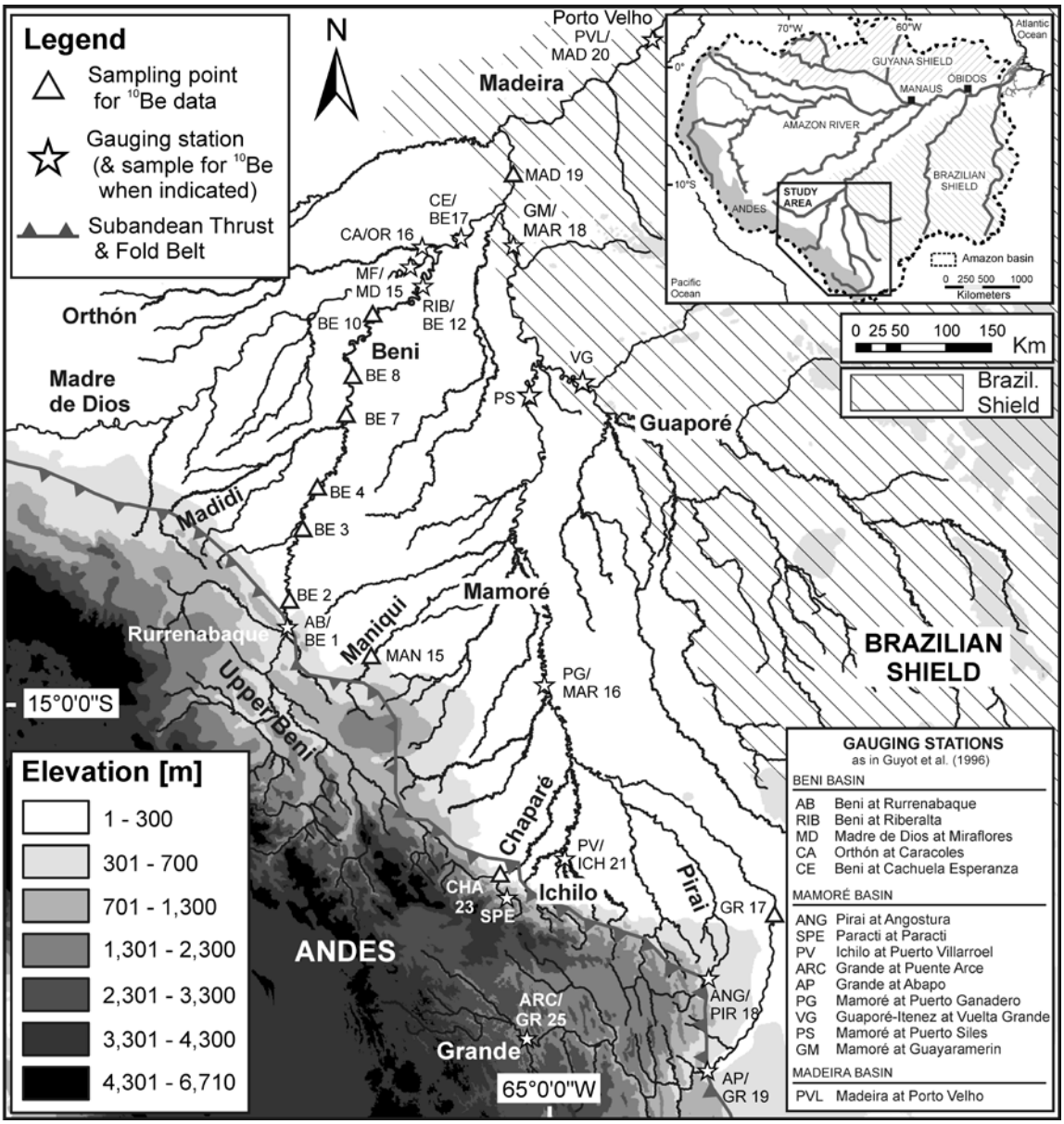

Figure 1) Detailed topographic map and fluvial network of the Beni and Mamoré River basins with sampling points for cosmogenic ^{10}Be (white triangles). Sediment gauging stations (white stars) operated by HYBAM are abbreviated as in Guyot et al. (1996). Where cosmogenic samples were taken at the same location as a gauging station, the sample name is indicated below the HYBAM gauging station code.

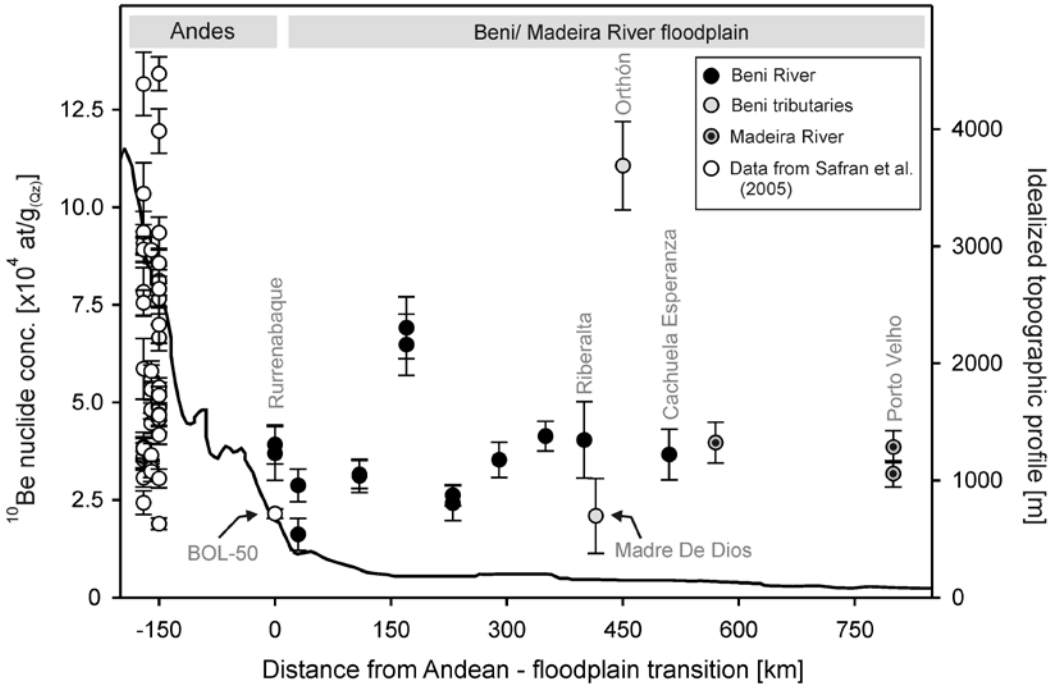

Figure 2) Cosmogenic nuclide concentration profile for the Beni (black circles) and Madeira River (grey circles with black dot) plotted against distance from transition between Andes and the floodplain at Rurrenabaque (km). Grey circles denote tributary samples. Right axis gives elevation of idealized topographic profile of the basin (m), which has been projected from several valley-perpendicular profiles into a single plane. Andean nuclide concentrations and nuclide concentration at Rurrenabaque (BOL-50) measured by Safran et al. (2005) are shown as white circles.

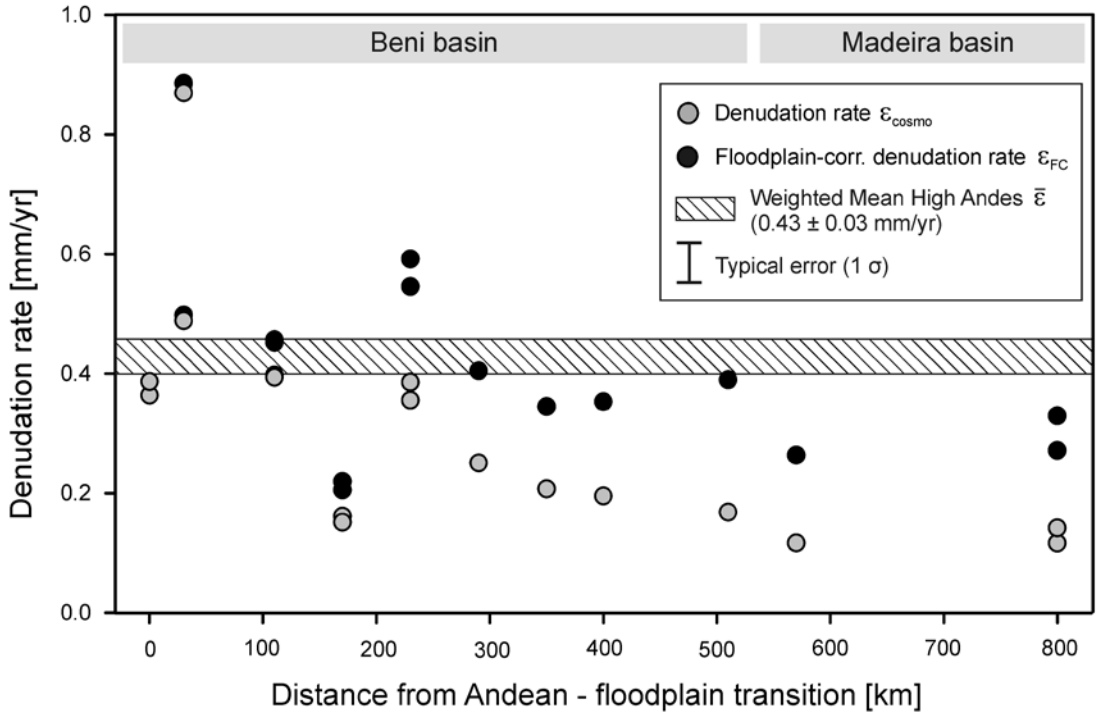

Figure 3) Cosmogenic nuclide-derived denudation rates for the Beni and Madeira basin, calculated using the production rate representative of each sampling points´ basin hypsometry (grey circles). For comparison, we extended the X-Axis to Porto Velho (PVL) on the Madeira River, whose basin also integrates over the Mamoré and Guaporé basins. Using a hinterland production rate of 15.3 at/$g_{(Qz)}$/yr, the cosmogenic denudation rates of the Beni River floodplain were recalculated (black circles, ε_{FC}) to exclude the artificial decrease in denudation rate caused by decreasing basin-averaged production rates away from sediment-producing areas (see text for more details). For Madeira River samples (downstream of > 550 km), we used a source area production rate of 12.9 at/$g_{(Qz)}$/yr for this correction. Horizontal bar denotes the flux-weighted Andean mean rate ($\bar{\varepsilon}$ = 0.43 ± 0.03 mm/yr) recalculated from Safran et al. (2005).

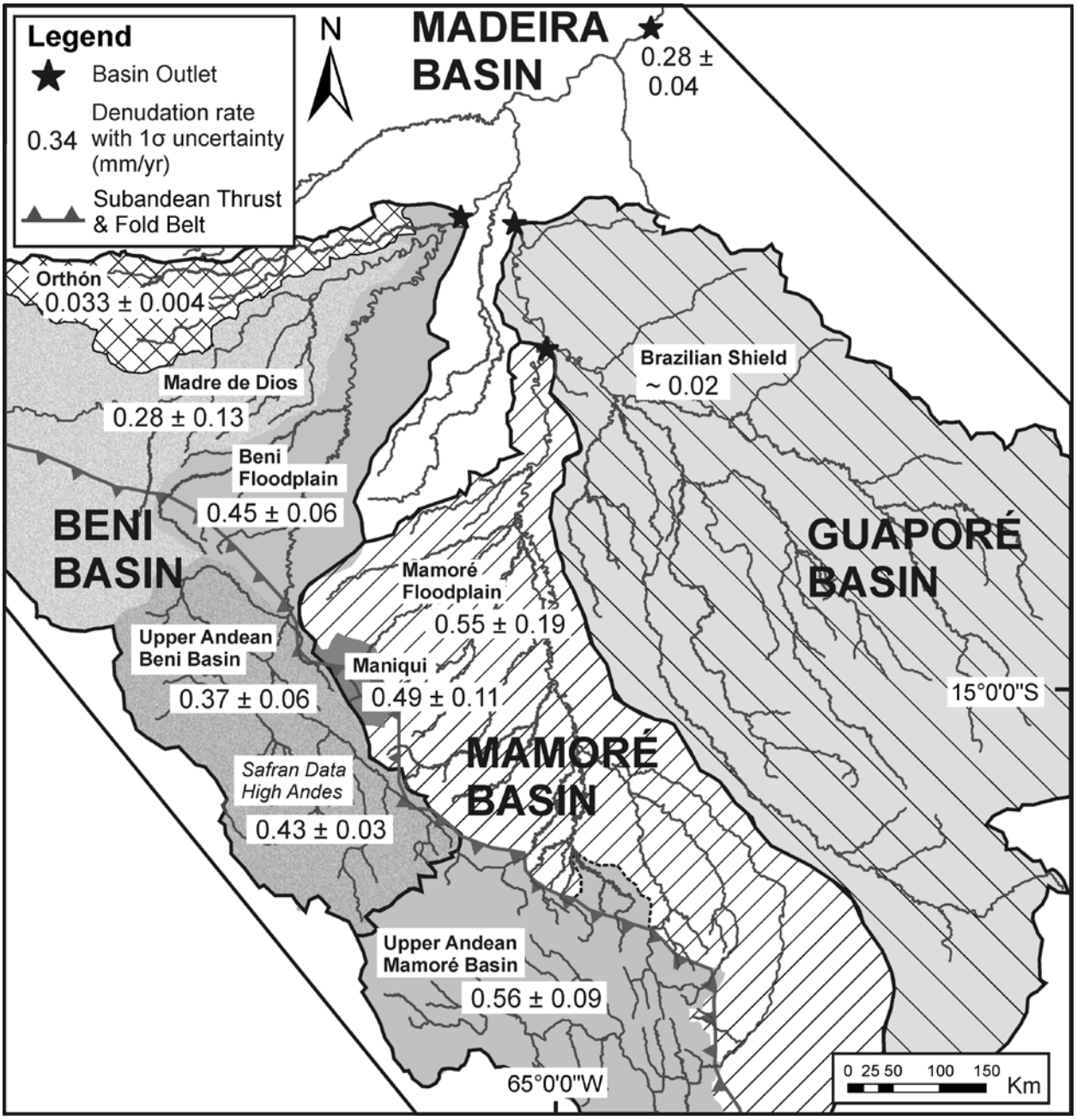

Figure 4) Cosmogenic nuclide-derived denudation rates (mm/yr) from Section 4 for tributaries of the Madeira basin including the Beni, Mamoré and Guaporé basins, of which their outlets are marked by black stars. The Beni basin is subdivided into its major tributaries of Orthón and Madre de Dios as well as the upper Andean part of the basin, for which an average denudation rate from sample BE 1 is given as well as the weighted mean recalculated from Safran et al. (2005). The Andean Mamoré basin includes the small Maniqui catchment and more southern Andean Mamoré samples of the Grande, Pirai, Ichilo, and Chaparé Rivers. The floodplain part of the Ichilo basin is indicated by the dashed line. An average denudation rate for the Brazilian Shield (~0.02 mm/yr) has been taken from Wittmann (2008).

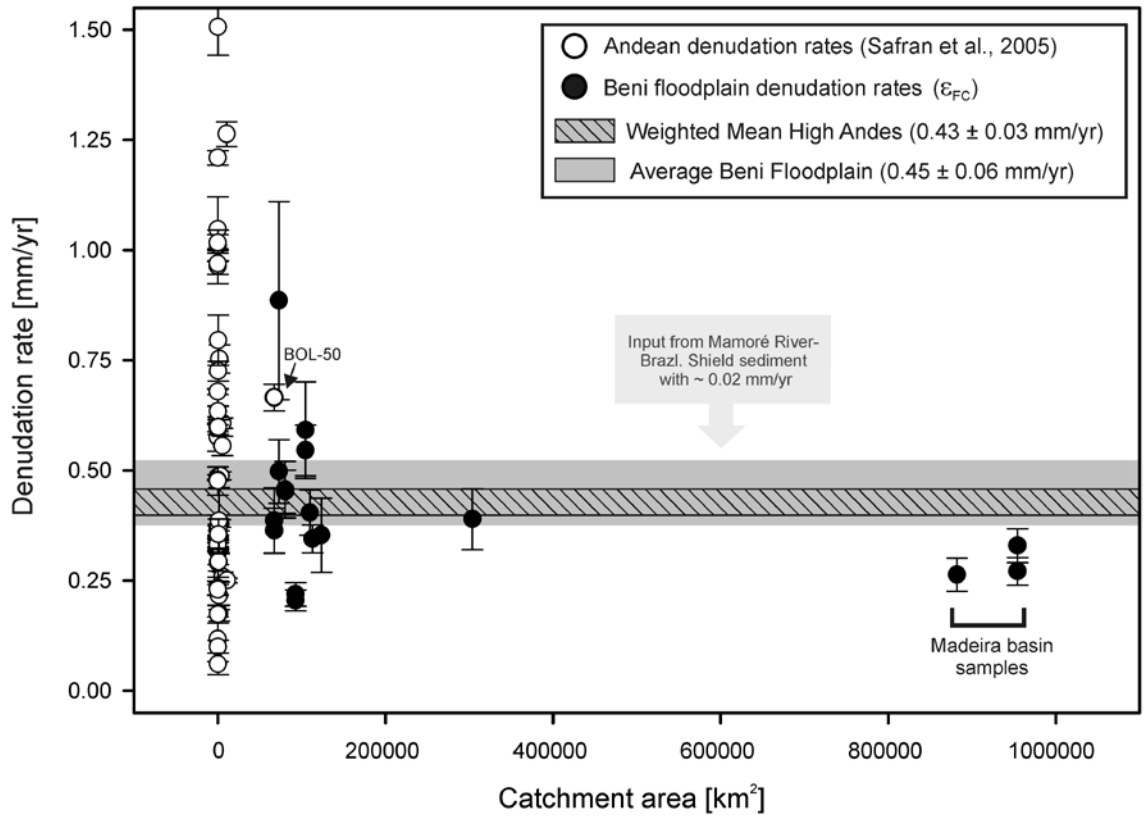

Figure 5) Denudation rates (with one sigma errors) for the Madeira basin at Porto Velho plotted against drainage area. Andean cosmogenic nuclide data is recalculated from Safran et al. (2005). Floodplain rates are corrected for decrease in production rate across low-elevation floodplain areas according to Eq. 1. The data shows that with increasing basin area, the spread in denudation rate decreases, and that the cosmogenic sample taken at 1.000.000 km^2 (Porto Velho) is similar to the Andean mean rate from Safran et al. (2005). The difference to the Andean average is in this case attributed to sediment input high in nuclide concentration from the slowly eroding parts of the Guaporé basin.

Table 1: Sample and basin characteristics and analytical results

Sample[a]	River/ location	Setting	Distance from Piedmont transition[b] [km]	Grain-size [µm]	Latitude[c] [°]	Longitude[c] [°]	Drainage area A_{basin}[d] [x10^4 km^2]	Andean sediment source area A_{FC}[d] [x10^4 km^2]	Basin-avg. mean altitude[d] [m]	^{10}Be concentration[e] [x10^4 at/g$_{(Qz)}$]	Total production rate[f] [at/g$_{(Qz)}$/yr]	Total production rate corr. for floodplain area P_{FC}[g] [at/g$_{(Qz)}$/yr]	Denudation rate ε_{cosmo}[h] [mm/yr]	Floodplain-corr. denudation rate ε_{FC}[i] [mm/yr]	Apparent age[j] [kyr]	Floodplain-corr. sediment load Q_{FC}[k] [Mt/yr]
Beni basin																
BE 1a	Beni at Rurrenabaque	Piedmont	0	125-250	-14.527	-67.497	6.8	6.8	2119	3.92 ± 0.50	15.3	-	0.36 ± 0.05	-	2.6	66
BE 1b	Beni at Rurrenabaque	Piedmont	0	250-500	-14.527	-67.497	6.8	6.8	2119	3.69 ± 0.69	15.3	-	0.39 ± 0.07	-	2.4	70
BE 2a	Beni	Floodplain	30	125-250	-14.284	-67.474	7.3	6.8	2094	2.87 ± 0.42	15.0	15.3	0.49 ± 0.08	0.50 ± 0.07	1.9	91
BE 2b	Beni	Floodplain	30	250-500	-14.284	-67.474	7.3	6.8	2094	1.62 ± 0.41	15.0	15.3	0.87 ± 0.22	0.89 ± 0.22	1.1	161
BE 3a-1	Beni	Floodplain	110	125-250	-13.571	-67.353	8.0	6.8	1921	3.13 ± 0.43	13.3	15.3	0.40 ± 0.06	0.46 ± 0.06	2.1	83
BE 3a-2*	Beni	Floodplain	110	125-250	-13.571	-67.353	8.0	6.8	1921	3.16 ± 0.36	13.3	15.3	0.39 ± 0.04	0.45 ± 0.05	2.1	82
BE 4a-1	Beni	Floodplain	170	125-250	-13.119	-67.185	9.3	6.8	1685	6.48 ± 0.79	11.3	15.3	0.16 ± 0.02	0.22 ± 0.03	4.2	40
BE 4a-2**	Beni	Floodplain	170	125-250	-13.119	-67.185	9.3	6.8	1685	6.91 ± 0.79	11.3	15.3	0.15 ± 0.02	0.21 ± 0.02	4.5	37
BE 7a	Beni	Floodplain	230	125-250	-12.512	-66.950	10.5	6.8	1511	2.42 ± 0.44	10.0	15.3	0.39 ± 0.07	0.59 ± 0.11	1.6	108
BE 7b*	Beni	Floodplain	230	250-500	-12.512	-66.950	10.5	6.8	1511	2.62 ± 0.27	10.0	15.3	0.36 ± 0.04	0.55 ± 0.06	1.7	99
BE 8a	Beni	Floodplain	290	125-250	-12.078	-66.882	11.0	6.8	1443	3.53 ± 0.45	9.5	15.3	0.25 ± 0.04	0.40 ± 0.05	2.3	74
BE 10a	Beni	Floodplain	350	125-250	-11.559	-66.677	11.3	6.8	1405	4.14 ± 0.38	9.2	15.3	0.21 ± 0.02	0.34 ± 0.03	2.7	63
BE 12a	Beni at Riberalta	Floodplain	400	125-250	-11.212	-66.249	12.4	6.8	1293	4.04 ± 0.98	8.5	15.3	0.19 ± 0.05	0.35 ± 0.08	2.6	64
MD 15a**	Madre de Dios at Miraflores	Floodplain	415	125-250	-11.112	-66.416	14.0	6.9	906	2.09 ± 0.96	6.4	-	0.28 ± 0.13	-	3.3	108
OR 16b	Orthón at Caracoles	Floodplain	450	250-500	-10.820	-66.110	3.2	3.2	236	11.06 ± 1.13	4.2[l]	-	0.033 ± 0.004	-	26.5	3
BE 17a	Beni at Cachuela Esperanza	Floodplain	510	125-250	-10.550	-65.600	30.4	6.8	960	3.66 ± 0.65	6.6	15.3	0.17 ± 0.03	0.39 ± 0.07	2.4	71
Mamoré basin																
GR 25a***	Grande near Puente Arce	Andes	-360	160-250	-18.609	-65.162	2.4	2.4	3321	14.24 ± 0.82	24.5	-	0.13 ± 0.01	- -	4.7	8
PIR 18b***	Pirai at Angostura	Piedmont	-65	250-500	-18.082	-63.457	0.16	0.16	1207	1.75 ± 0.40	7.8	-	0.40 ± 0.10	- -	2.2	2
PIR 18c***	Pirai at Angostura	Piedmont	-65	500-800	-18.082	-63.457	0.16	0.16	1207	1.32 ± 0.55	7.8	-	0.54 ± 0.23	- -	1.7	2
GR 19b**	Grande at Abapo	Piedmont	0	250-500	-18.909	-63.410	6.0	6.0	2501	2.47 ± 0.32	20.1	-	0.63 ± 0.09	- -	1.2	101
CHA 23a**	Chaparé at Villa Tunari	Piedmont	0	125-250	-16.974	-65.414	0.49	0.49	2413	5.88 ± 0.73	20.2	-	0.26 ± 0.03	- -	2.9	3
MAN 15b**	Maniqui at San Borja	Piedmont	18	250-500	-14.864	-66.738	0.53	0.53	865	1.16 ± 0.28	6.5	-	0.49 ± 0.11	- -	1.7	7
ICH 21a**	Ichilo at Puerto Villarroel	Piedm./Floodpl.[m]	70	125-250	-16.841	-64.787	0.76	0.46	678	1.65 ± 0.34	5.6	-	0.33 ± 0.07	- -	3.0	7
GR 17b**	Grande at Puerto Pailas	Floodplain	190	250-500	-17.655	-62.777	8.1	7.1	2104	2.77 ± 0.49	14.5	18.3	0.42 ± 0.08	0.51 ± 0.09	1.5	99
MAR 16a***	Marmoré at Puerto Ganadero	Floodplain	405[n]	160-250	-14.864	-64.990	15.9	12.3	956	1.32 ± 0.42	6.5	11.4	0.47 ± 0.15	0.72 ± 0.23	1.2	239
MAR 16b***	Marmoré at Puerto Ganadero	Floodplain	405[n]	250-400	-14.864	-64.990	15.9	12.3	956	0.96 ± 0.37	6.5	11.4	0.64 ± 0.26	0.99 ± 0.38	0.8	329
MAR 18a-1	Marmoré at Guayaramerin	Floodplain	560[n]	125-250	-10.808	-65.346	59.9	12.3	448	4.67 ± 1.06	4.5	11.4	0.09 ± 0.02	0.20 ± 0.05	4.1	67
MAR 18a-2**	Marmoré at Guayaramerin	Floodplain	560[n]	125-250	-10.808	-65.346	59.9	12.3	448	5.33 ± 2.08	4.5	11.4	0.08 ± 0.03	0.18 ± 0.07	4.7	59
Madeira basin downstream of Beni-Mamoré confluence																
MAD 19a	Madeira at Ribeirao	Floodplain	570[o]	125-250	-10.229	-65.281	88.2	26.0	594	3.97 ± 0.52	5.0	12.9	0.12 ± 0.02	0.26 ± 0.04	3.1	185
MAD 20a-1*	Madeira at Porto Velho	Floodplain	800[o]	125-250	-8.770	-63.909	95.4	26.0	560	3.87 ± 0.41	4.9	12.9	0.12 ± 0.01	0.27 ± 0.03	3.0	190
MAD 20a-2*	Madeira at Porto Velho	Floodplain	800[o]	125-250	-8.770	-63.909	95.4	26.0	560	3.18 ± 0.34	4.9	12.9	0.14 ± 0.02	0.33 ± 0.04	2.5	231

*^{9}Be carrier added to these samples contains a ratio of ^{10}Be/^{9}Be of 1.25 ± 0.41x10^{-14}. **In these cases the ratio of ^{10}Be/^{9}Be is 2.35 ± 1.08x10^{-14}. ***In these cases the ratio of ^{10}Be/^{9}Be is 1.10 ± 0.66x10^{-14}.

[a] "a" and "b" denote different grain size fractions, and "1" and "2" denote lab replicates.
[b] Negative distances denote distances upstream of transition zone (Andean area).
[c] Reference frame is UTM coordinate system.
[d] Derived from GIS analysis using spatial grid resolution of 1 km.
[e] Corrected for blank, with combined analytical and blank error.
[f] Total production rate, calculated for fast and slow muonic and nucleogenic components after Dunai (2000).
[g] Source area production rate excluding floodplain area.
[h] Combined errors on ^{10}Be measurement, blank, and 5% production rate error due to shielding and spatial resolution effects.
[i] Recalculated denudation rate with hinterland production rate.
[j] Gives time spent in upper ~60 cm of eroding layer, calculated with the floodplain-corrected denudation rate where possible.
[k] Calculated from floodplain-corrected denudation rate, or, for floodplain-area free basins, with normal denudation rate using a mean density of 2.7 g/cm^3.
[l] Production rate corrected for paleomagnetic intensity changes.
[m] At the sampling point, the basin integrates over ~39% of floodplain area.
[n] Distance measured along Mamoré main channel.
[o] Distance measured along Beni main channel.

Table 2: Sediment gauging data

Gauging station[a]	River/ Location	Setting	Drainage area A_{basin} [$\times 10^4$ km^2]	Andean sediment source area A_{FC} [$\times 10^4$ km^2]	Gauging period [yr]	Suspended sediment load Q_S [Mt/yr]	Specific dissolved load Q_D [Mt/yr]	Total sediment load Q_M [Mt/yr]	Total sediment yield F_M [t/km^2/yr]	Denudation rate ε_M[b] [mm/yr]	Floodplain-corrected total yield F_{MFC} [t/km^2/yr]	Floodplain-corrected denudation rate ε_{MFC}[c] [mm/yr]
Beni basin												
AB	Beni at Rurrenabaque	Piedmont	6.8	-	1969-1990	212	5.2	217[d]	3181	1.18	-	-
RIB	Beni at Riberalta	Floodplain	11.9	6.8	1983-1990	122	8.2	130	1054	0.39	1920	0.71
MF	Madre de Dios at Miraflores	Floodplain	12.4	6.9	1983-1990	71	11	82	610	0.23	-	-
CA	Orthón at Caracoles	Floodplain	3.2	-	1983-1990	2	0.9	3	70	0.03	-	-
CE	Beni at Cachuela Esperanza	Floodplain	28.3	6.8	1983-1990	191	20	210	714	0.26	3120	1.15
Mamoré and Guaporé basin												
ARC	Grande at Puente Arce	Andes	2.4	-	1969-1974	136	-	136	5730	2.12	-	-
ANG	Pirai at Angostura	Piedmont	0.14	-	1976-1985	3	-	3	2080	0.77	-	-
SPE	Paracti at Paracti	Piedmont	0.03	-	1972-1973	4	-	4	10940	4.05	-	-
AP	Grande at Abapo	Piedmont	6.0	-	1976-1990	138	5	143	2390	0.89	-	-
PV	Ichilo at Puerto Villarroel	Floodplain	0.76	0.46	1983-1990	9	1	10	1260	0.47	2160	0.80
PG	Mamoré at Puerto Ganadero	Floodplain	15.9	12.3	1983-1990	64	9	73	428	0.16	590	0.22
PS	Mamoré at Puerto Siles	Floodplain	21.6	12.3	1983-1990	47	14	61	251	0.09	495	0.18
GM	Mamoré at Guayaramerin	Floodplain	59.9	12.3	1983-1990	66	17	83	123	0.05	672	0.25
VG	Guaporé-Itenez at Vuelta Grande	Floodplain	35.4	-	1983-1990	2	3	4	9	0.003	-	-
Madeira basin												
PVL	Madeira at Porto Velho	Floodplain	95.4	26.0[e]	1978-1993	230[f]	-	230	241	0.09	883	0.33

[a] As indicated in Figure 1; all sediment load data is from Guyot et al. (1996).
[b] Calculated with a mean density of 2.7 g/cm^3 and the drainage area in km^2.
[c] Recalculated with Andean hinterland area.
[d] An estimation of Maurice-Bourgoin et al. (2002) amounts to 300 Mt/yr at this location, which corresponds to a denudation rate of 1.63 mm/yr.
[e] Includes Andean Beni, Madre de Dios, and Andean Mamoré area.
[f] From Guyot et al. (1999).